Deutscher Luft- und Raumfahrtkongress 2022
DocumentID: 570387

FAST AND ROBUST OPTIMIZATION OF UNMANNED AERIAL VEHICLE LOCATIONS CONSIDERING RESTRICTED AREAS

H. Braßel, T. Zeh, H. Fricke
Technische Universität Dresden, Chair for Air Transport Technology and Logistics, Dresden, Germany

Abstract

Unmanned Aerial Vehicles (UAV) enable swift and autonomous response to urgent needs, such as search & rescue missions or material delivery. At the same time, airspace restrictions are being established to reduce the external risk of UAV operation considering air and ground risk, which may hinder the efficient usage of UAV in combination with their range-limiting battery capacity. In this study, we present a robust optimization model for a facility location problem of UAV hangars, considering demand hotspots, restricted areas, a standard mission to satisfy battery capacity constraints, and the impact of wind scenarios using water rescue missions as an example. We use open source GIS data to derive positive and negative location factors for UAV hangars and areas of increased risk of drowning as demand points. The pathfinding for the UAV mission uses an A* algorithm to find the shortest mission trajectories in five different restriction scenarios. In addition, binary occupancy grids and image processing algorithms identify restriction-free connections for faster computation. For the optimal UAV hangar locations, we maximize accessibility while minimizing the service time to the demand points showing an improvement of the average service time of 624.20 s for all facility candidates to 401.69 s for one and 315.38 s for two optimal facilities, respectively.

Keywords

Unmanned Aerial Vehicle; Facility Location Problem; Mission Planning; Restricted Airspace; Search & Rescue

1. INTRODUCTION

According to the World Health Organization [1], drowning is the third leading cause (7%) of unintentional injury-related deaths worldwide. The 2021 DLRG annual report [2] shows that around 85% of all victims in Germany drowned in inland waters. Therefore, alerting emergency responders and localizing victims in the water constitute particular challenges within the rescue chain. Autonomous Unmanned Aircraft Systems (UAS) for Search & Rescue (SAR) operations may detect persons in distress faster than helicopters, boats, or lifeguards. Furthermore, the precise dropping of a flotation device may extend the chance of survival until conventional rescue service arrives. However, it also requires safe integration into the airspace, well-suited operation automation, and ensuring the safety of third parties on the ground.

The research project RescueFly studies the prototypical implementation of two non-holonomic THOLEG[1] Unmanned Aerial Vehicle (UAV) for inland water SAR at the remote Lusatian Lake District located in the federal state of Brandenburg and the Free State of Saxony in Germany. The UAVs will act automatically once an emergency call with an initial search location has been raised. Thereby, RescueFly covers all elements from UAS and intelligent UAV hangar development, safe and efficient mission planning, autonomous detection of persons in distress, automatic dropping of flotation devices, and the operational integration in the existing rescue chains of the two federal states.

This paper focuses on the determination of optimized locations for decentralized autonomous UAV considering areas with increased potential for incidents (hotspots), standard mission profiles respecting flight restriction zones and potentially crowded areas, and requirements for the UAV hangar location. For this purpose, we discretize and merge 109 geo-referenced layers from open data sources to determine the solution space, plan safe flight routes, and solve the Uncapacitated Facility Location Problem (UFLP) given two finite sets of potential hangar locations and hotspots. The geo-referenced data are transformed into a binary occupancy grid image and labeled using a fast connected-component algorithm to identify non-permissible connections between potential UAV hangar locations and hotspots to reduce computational effort during the path search. In addition, direct connections, i.e., paths not affected by restrictive areas, are identified using a fast ray-occupancy-intersection algorithm. Finally, the A* algorithm served to compute all remaining paths. Since battery capacity constrain the UAV mission, the accessibility and service time are determined considering a standard SAR mission and a save return to the UAV hangar.

This paper continues with a review of the state of the art, focusing on other SAR applications for UAS, UAV mission planning, automated detection of persons in distress, and UAS Facility Location Problem (FLP). The following chapter then describes the methodology to solve the

[1] https://tholeg.com/

doi: 10.25967/570387

UAV facility location problem in a multi-objective optimization, considering positive and negative location factors and constraints like battery capacity and external risk for up to two locations as an example. Subsequently, the results of our work are shown, indicating candidate locations for the UAV hangars. Finally, an outlook on the next steps in the RescueFly project concludes the paper.

2. STATE OF THE ART

2.1. SAR Concepts with UAS

Various SAR concepts have been studied using UAS as a component in the rescue chain. Ajgaonkar et al. [3] developed a UAV to assist lifeguards at coastal beaches. They assumed that the lifeguard provides the initial identification of the person in distress to a UAVoperator, who then searches the area to drop a flotation device. Similarly, Seguin et al. [4] conducted a study with UAV delivering flotation devices to swimmers at the lifeguard's remote control, showing that the faster delivery compared to the lifeguard or a jetski reduces the submersion time and therefore the risk of drowning significantly. Dufek and Murphy [5] introduced a concept of combining an UAV with an autonomous Unmanned Surface Vehicle (USV) for offshore emergencies, which searches the person in distress and serves as a flotation device. The UAV serves to first guide the USV to the victims and then to track the drift of USV for the emergency responders.

Liu et al. [6] presented an operational concept for UAV usage in SAR missions over rivers, in which they predicted the drift to delimit the search area using Monte-Carlo simulations. For the faster coverage of larger areas, authors like Ruetten et al. [7] proposed swarm networks consisting of many UAVs that organize themselves to reach optimal coverage with minimal overlapping. While this approach ensures fast detection over large areas, it poses an additional external risk to persons and significantly increases the required infrastructure and equipment. Thus, it is deemed unfeasible for SAR missions at bathing lakes.

2.2. UAV Flight Path Planning for SAR

The most crucial factor in SAR is the time since the early detection of a drowning person substantially improves the chances of survival. Additionally, the battery capacity limits the flight time of an UAV, which requires efficient path planning from the UAS facility to identify, reach and search the target area. Brühl et al. [8] provided a methodology to estimate energy consumption based on the flight phase for various large air taxis, including multi-copter designs similar to UAVs for SAR. Chu et al. [9] analyzed the impact of wind on the battery capacity for small quad-copter UAV, considering wind speed, direction, and turbulence in a simulation. They found wind conditions up to $11\,\mathrm{m\,s^{-1}}$ suitable for surveying crash areas regarding the additional energy consumption, although higher turbulence significantly increases their consumption.

Lin and Goodrich [10] created a probability distribution map to accelerate wilderness SAR with a UAV flying $60\,\mathrm{m}$ above ground. With the map, they converted the path search into a discretized combinatorial optimization problem and applied variants of Complete-coverage, Local Hill Climbing, and Evolutionary algorithms with and without a defined destination, finding that the Local Hill climbing algorithm with a convolution kernel performs best. Hayat et al. [11] developed a multi-objective path planning based on a genetic algorithm that minimizes the search time, which balances the search area coverage with the network connectivity coverage to ensure communication to the emergency responders. Wang et al. [12] proposed a vortex search algorithm for multi-objective path optimization to guide UAV to forest fires, considering obstacles and terrain described with a cubic interpolation method.

After reaching the search area, an efficient method for sweeping this area is required. Zuo et al. [13] suggested an extended square search, which expands from the center of the search area, assuming that positions closer to the center are more likely than distant ones. Liang et al. [14] developed a heuristic to avoid redundant image coverage and maximize image quality during a SAR mission with an energy-constrained UAV. Dakulović et al. [15] developed a complete coverage D* algorithm for a floor-cleaning mobile robot, minimizing path length and search time in a constrained space with unknown obstacles. Xu et al. [16] studied a Complete Coverage Neural Network (CCNN) for an unmanned surface vehicle for complete coverage of a search area and combined it with an improved A* algorithm to escape deadlock situations efficiently. Sun et al. [17] proposed a two-step auction method to coordinate multiple UAV to cover a mutual search area, considering the avoidance of obstacles and the energy constraints of the UAV.

2.3. Automated Detection of a Person in Distress

When covering the search area with the UAV, the person in distress must be detected swiftly and automatically, even when large groups of persons are swimming at the same time. For this, Qingqing et al. [18] analyzed different altitudes and camera angles for human detection in marine SAR to find a trade-off between speed and detection accuracy with the real-time object detection model of YOLOv3. They found that persons can be detected farther away the closer the camera angle is to facing straight down. Above $100\,\mathrm{m}$, however, the confidence and accuracy drop since it is a function of the camera lens and image resolution. Rudol and Doherty [19] presented a method to detect human bodies lying or sitting on the ground by combining video and thermal sensors. For maritime SAR, it remains unclear if a thermal sensor can produce similar results, especially for submerged persons. Bejiga et al. [20] trained a Convolutional Neural Network (CNN) to assist avalanche SAR with a faster detection of victims utilizing optical cameras fitted to UAV. Lygouras et al. [21] used CNN to detect persons swimming in open water for an autonomous UAV. Feraru et al. [22] proposed a concept to deploy autonomous UAV for man-overboard incidents using a probabilistic leeway model with a Faster Region-based Convolutional Neural Network (R-CNN) to detect the person in the water. Liu and Szirányi [23] studied a two-stage approach, in which they first detected persons in UAV video footage and then interpreted basic gestures used by persons in distress using neural networks. Wang et al. [24] proposed a different two-stage approach. First, persons are located with simpler features to reduce the search space, and second, a CNN is applied to the previously selected areas.

2.4. Facility Location Problem

A FLP models the selection and localization of facilities to serve demand at specific points or areas, e.g., for applications like hospitals, fire stations, or warehouses. The UFLP is one of the most commonly considered combinatorial optimization problems, in which two finite sets of potential facilities and demand points are considered by assessing the associated costs for the facility construction and the distance or cost for each combination of demand point and facility location. The objective of the optimization problem is to select the facility locations to be established and allocate the demand points by minimizing the total operational costs [25, 26]. The k-facility problem is a UFLP with the additional constraint of $k \in \mathbb{N}$ facilities being allowed to open. For facility construction costs equal to zero, k-median clustering can be applied to determine centroids as facility locations. This approach, however, assumes that all distances are as the crow flies [27]. Another option is the lower-bounded FLP, e.g., with the algorithm of Ahmadian and Swamy [28], where each facility must serve a certain minimum amount of demand.
For UAV delivering first-aid products, Zhu et al. [29] developed a two-stage FLP approach for robust optimization considering customers demand uncertainty. They proposed three models for the problem that outperform a deterministic FLP. Lynskey et al. [30] studied the distribution of UAV ground facilities. They solved the problem with k-means clustering while adding the energy consumption of the UAV as costs using a traveling salesman algorithm to enable UAV to perform multiple tasks with one flight. According to our understanding, restricted areas for the UAV, such as the UAS geographic zones according to the Commission Implementing Regulation (EU) 2019/947 [31] and § 21h LuftVO [32], have not been considered in a FLP problem for UAV yet. These regulations, however, impact the routing significantly as they aim to reduce external risk. In some cases, they may prohibit the placement of a UAV hangar entirely, so it should be included in the FLP problem and the related mission planning.

3. METHODOLOGY

3.1. Overview of the Approach

The RescueFly concept of operations plans to assist SAR missions at Geierswalder Lake and Partwitzer Lake utilizing automated UAS located in decentralized hangars. For this, the hangar location(s) should provide minimal service time to hotspot areas where increased accidents are expected due to their geographic characteristics and nearby amenities while considering positive and negative hangar location factors. For this purpose, the shortest restriction-free flight trajectories from all candidate locations to all hotspots are computed, considering national and European regulations and external risk factors like potentially crowded areas, to identify the location(s) serving all hotspots while minimizing their service time. For this, this paper utilizes open source data to determine an optimal location of the UAV hangar. FIG 1 summarizes the approach. The input and output of each step are indicated by the green and blue colors, respectively.

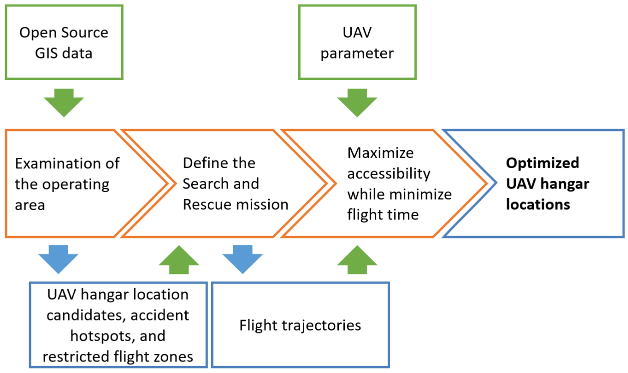

FIG 1. Overview of approach

A hangar facility must provide solid ground, electricity supply, and reasonable access for installation and maintenance of the system. Furthermore, the communication must not be shaded by vegetation or located within restrictive areas (e.g., hazard areas, flight restriction zones, natural reserves). At the same time, designated beaches, recreation sites, hotel and camping facilities, grasslands, and other facilities where people are engaged in activities adjacent to lakes, e.g., barbecue areas, boat slipways, and boat rentals, increase the intrinsic risk for accidents in water bodies. When planning a SAR mission, the risk to uninvolved parties, here the air and ground risk, must be considered. SAR operations are excluded from the remit of Regulation (EU) 2018/1139 [33], which means that the competent national authority is responsible for regulating SAR operations. According to § 21k LuftVO [32], authorities conducting SAR operations are permitted to fly through UAS geographical zones defined by EU 2019/947 [31] and § 21h LuftVO [32]. As the UAV hangar locations should provide a robust and optimal solution concerning various restrictive flight areas to decide on complying with or flying through UAS geographical zones as an operational decision, e.g., depending on the urgency or the exposed crowd size at beaches. For this purpose, this paper considers five different scenarios:

1) Restriction-free flight from the hangar to the hotspot invoking the special rights of authorities conducting SAR missions according to § 21k LuftVO [32];
2) Compliance with specified air risk relevant UAS geographical zones according to EU 2019/947 [31] and § 21h LuftVO [32], e.g. required distance to airfields;
3) Compliance with specified air and ground risk relevant UAS geographical zones;
4) Compliance with all specified UAS geographical zones; and

Key	Value(s)
landuse	grass, greenfield
natural	grassland, heath, srub, scree

TAB 1. OSM map features for positive UAV hangar location factors

5) Compliance with all specified UAS geographical zones and additional avoidance of potentially crowded areas.

Furthermore, the solution should be robust against wind effects. Therefore, different wind scenarios are considered for each of the above scenarios.

3.2. Acquisition of Open Source Data

This section reviews open source data to retrieve relevant information for UAV hangar location evaluation, divided into three georeferenced data requirements groups. First are positive and negative location factors for constructing UAV hangars. Second, data serve to identify areas of high intrinsic risk for a waterside accident or incident. Moreover, third, data describing the UAS geographic zones according to EU 2019/947 [31] and § 21h LuftVO [32] to be avoided during mission planning, minimizing the external risk and environmental impact. The primary source for the former two is the OpenStreetMap (OSM)[2], a community-driven database for georeferenced data layers. OSM defines the georeferenced data with nodes, ways, and relations to describe the geometry, supplemented by tags (key-value principle) describing the object's function. Using Overpass API[3], it is possible to define queries for extracting data based on region, layers, and tags.

The location factors are defined based on the surface and its ability to accommodate a UAV hangars. As listed in TAB 1, six tags for areas with grass and minimal vegetation are considered positive. Eight tags for areas with forest, large amounts of trees, or wetlands will require additional construction work or shading effects for communication, expressed with a negative location factor according to TAB 2. Furthermore, we assume that each potential UAV hangar location requires road access (24 values included from the highway tag) with a maximum permitted distance of 20 m from the road. In addition, the UAV hangar cannot be established on water surfaces, provided as Web Map Service (WMS)[4]. Finally, the availability of power supply should be another positive location factor, but the required data is not public.

TAB 3 shows 34 map features representing hotspot indicators. We assume that these features induce a higher probability of an incident or accident near water bodies. For this purpose, we extrude the resulting map feature nodes and areas by a radius of $150\,\mathrm{m}$ in size, followed by an intersection with the water surfaces in the area under investigation. Areas that are subsets of the extruded hotspot indicators and subsets of the water areas result

[2]https://www.openstreetmap.org/

[3]https://overpass-turbo.eu/

[4]https://geoportal.brandenburg.de/de/cms/portal/start

Key	Value(s)
boundary	forest, forest_compartment, hazard
landuse	forest
natural	tree, tree_row, wood, wetland

TAB 2. OSM map features for negative UAV hangar location factors

Key	Value(s)
amenity	boat_rental, boat_sharing, ferry_terminal, public_bath, parking, parking_space, lounger
building	beach_hut
emergency	lifeguard, life_ring, phone
landuse	grass
leisure	marina, slipway, swimming_area, swimming_pool, water_park, beach_resort, park, picnic_table
lifeguard	tower
man_made	pier
natural	beach, shingle, shoal, sand
sport	sailing, swimming, surfing, wakeboarding, water_polo, water_ski
tourism	camp_site, caravan_site

TAB 3. OSM map features for hotspot areas

in the hotspot areas. The radius of $150\,\mathrm{m}$ is determined from the distance between buoys and shore of approximately $120\,\mathrm{m}$ plus an additional $30\,\mathrm{m}$, since the OSM features may georeference slightly outside water areas. We assume that most swimmers tend to keep within the prescribed limits, increasing the risk of accidents in these areas.

For the flight path planning of the standard SAR mission, data concerning UAS geographic zones [31, 32] is required. Theoretically, § 21k LuftVO [32] permits public safety agencies to operate in UAS geographic zones, e.g, for SAR missions. However, this works aims to minimize both ground and air risk. Thus, we implemented different scenarios in the FLP to consider varying constraints to the path-finding process to study the impact of the geographic zones. For the operation of UAV in Germany, the Digital Platform for Unmanned Aviation (dipul) provides a map tool[5] and web map service which provides the UAS geographic zones defined as separated layers. For the transmission of data, the availability of a sufficient boardband connection should be considered as well. However, the so-called Breitband-Monitor[6] of the German Bundesnetzagentur provides only coverage at ground level, so open-source data at cruising and search altitude cannot be retrieved.

[5]https://maptool-dpul-prod.dfs.de/

[6]https://www.breitband-monitor.de/mobilfunkmonitoring

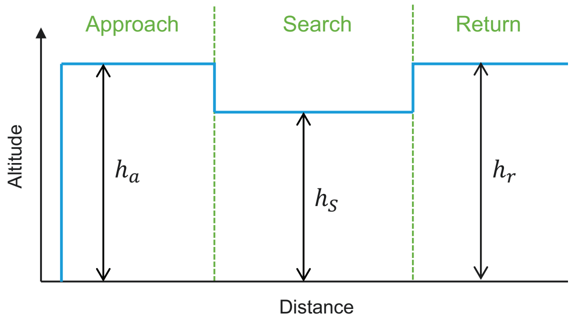

FIG 2. Vertical profile of the standard SAR mission divided into the approach from the UAV hangar to the hotspot area, the search to cover the whole hotspot area and the return to the UAV hangar

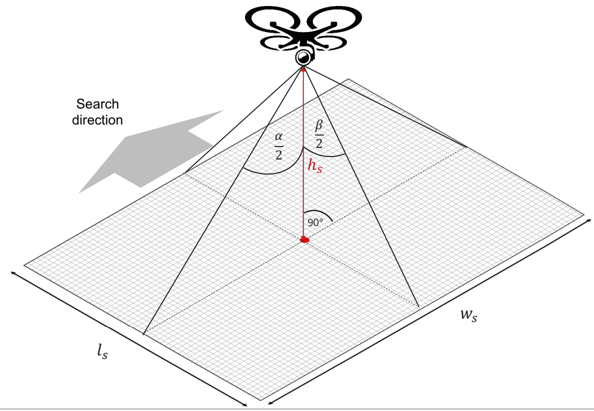

FIG 3. Covered surface in one frame during search given with search width w_s and length l_s as a function of the camera's lateral and vertical field of view (α and β, respectively) for a defined search altitude h_s

3.3. Definition of the standard SAR Mission

As the battery capacity limits the operation duration of the UAV, a restriction-free flight path between each potential UAV hangar location and each hotspot, and a standard search mission must be defined to assess the accessibility of the hotspot and feasibility of the search mission, given varying UAS geographic zones and wind scenarios. Each standard SAR mission consists of three components the approach, the search mission, and the return flight. For a consistent consideration, we assume that the approach and return flights have the same horizontal and vertical profiles. Furthermore, as shown in FIG 2, we assume a vertical climb at the UAV hangar to the approach altitude h_a, which is maintained until the UAV reaches the hotspot area. There, the UAV descends vertically to the search altitude h_s, which depends on the required resolution to detect a person in distress, and continues the flight with a search pattern at constant h_s. After the search, the UAV climbs, maintaining the return altitude h_r until reaching the origin.
A constant altitude of $h_a = h_r = 100\,\text{m}$ above ground is assumed for approach and return, leaving a safety buffer to the maximum permitted altitude of $120\,\text{m}$ according to 'specific' category [31]. h_s depends on the characteristics and orientation of the camera and the required resolution for the automated detection of a person in distress. The camera of our UAV has an aspect ration of $4:3$ with a resolution of $R = 12\,\text{Mpx}$, a lateral field of view $\alpha = 56°$ and a vertical field of view $\beta = 45°$. The camera is facing down perpendicular to the water surface, guaranteeing the best coverage and detection [18]. Furthermore, the larger α is perpendicular to the search direction so that the UAV is centered above the middle of the covered surface in a single camera frame, as shown in FIG 3. Then, the achieved pixel density D in [$\text{px}\,\text{m}^{-2}$] per frame is given with the search width w_s and length l_s in [m] according to:

$$D = \frac{R}{w_s \cdot l_s} \tag{1}$$

Using the tangent of two assumed right-angle triangles, w_s and l_s can be determined at given h_s utilizing the camera parameters α and β:

$$w_s = 2 \cdot h_s \cdot \tan(0.5 \cdot \alpha) \tag{2}$$

$$l_s = 2 \cdot h_s \cdot \tan(0.5 \cdot \beta) \tag{3}$$

The required minimum pixel density D_{min} significantly drives the optimal h_s to detect persons in distress autonomously. A trade-off is necessary between a high-as-possible h_s for minimum-time coverage of the search area and thus fast SAR and a sufficiently high pixel density to solve the detection and recognition task, i.e., to distinguish persons in distress from all other swimmers. For estimating D_{min}, a set of test images of 35 swimming volunteers has been taken at Lake Partwitz under sunny and clear conditions without any significant wind. From the set, 96 images of different pixel densities between 5 to $3300\,\text{px}\,\text{m}^{-2}$ have been generated and presented to 10 test persons (3 female, 7 male) aged 30 to 40 ($\mu = 33.4, \sigma = 3.34$),thus equals 960 samples. The test person's tasks are (a) detecting objects in the image and (b) recognizing and describing the activity of the swimming persons. If all persons per image are detected, task (a) is classified as positive; if at least one person remains undetected, it is considered negative. If the test persons describe all activities of the swimmers correctly (e.g., breaststroke with drawn legs), task (b) is classified as positive. The experiments show an average $D_{min,(a)} = 9\,\text{px}\,\text{m}^{-2}$ ($\sigma_{(a)} = 8$) and $D_{min,(b)} = 503\,\text{px}\,\text{m}^{-2}(\sigma_{(b)} = 493)$. The task complexity strongly correlates with the number and types of objects per test image resulting in high standard deviations. Thus, images containing few volunteers or volunteers on floating objects (e.g., surfboards) show significantly lower D_{min} due to contrast and size. Also, their activities are recognized more reliably than images with many volunteers swimming closely together. The obtained D_{min} from the test persons serve as estimates for the Deep Convolutional Neural Network (DCNN) intended to automatically detect a person in distress, assuming it will not perform significantly better or worse than humans. van Dyck et al. [34] confirm this hypothesis, in which the DCNNs ResNet18 and vNet achieved 79.05% and 84.76% accuracy, respectively, compared to 89.96% of human observers. With D_{min}, eqs. (1) to (3) are rearranged to solve for h_s:

$$h_s \leq \sqrt{\frac{R}{4 \cdot D_{min} \cdot \tan(0.5\alpha) \cdot \tan(0.5\beta)}} \tag{4}$$

Since the goal of the search mission is the reliable recognition of the person in distress, it is assumed that $D_{min} = D_{min,(b)} + 3\sigma_{(b)} = 1981$ is required to avoid misdetection. With eq. (4), $h_s \leq 82.92\,\mathrm{m}$ is determined to fulfill the task (b).

With the standard UAV mission, a set can be generated from the potential UAV hangar location F (Facility), a hotspot D (Demand), a wind scenario W, and a geographic zone scenario Z. The corresponding total flight time $t_{i,j}^{m,n} \in \mathbb{R}+$, for $i \in F$, $j \in D$, $m \in W, n \in Z$ constitutes the evaluation metric. The flight distance $d_{i,j}^{n}$ results from the shortest restriction-free flight path from $i \in F$ to $j \in D$ considering $n \in Z$. For this, the approach and return flight are assumed identical, i.e., $d_{i,j}^{n} := d_{j,i}^{n}$. Since various shapes of hotspot areas exist and the search time depends on the coverage algorithm, we assume a simplified rectangular hotspot area a_j [m^2] with edge length w_s [m] of FIG 3 and add a detour factor $k = 1.1$ to account for different coverage algorithms and shapes, resulting in a search distance s_j:

$$s_j = k \cdot \left(\frac{a_j}{w_s} - l_s\right) \tag{5}$$

According to the manufacturer, a reliable cruise speed during approach and return $v_1 = 10\,\mathrm{m\,s^{-1}}$ and a vertical rate $v_2 = 2.5\,\mathrm{m\,s^{-1}}$ is achieved. During the search phase, we assume slower search speed $v_3 = 5\,\mathrm{m\,s^{-1}}$ to provide suitable coverage and reduced motion blur. The total flight time for successive maneuvers (cf. FIG 2) is:

$$t_{i,j}^{m,n} = \left(2\frac{h_a}{v_3} + 2\frac{d_{i,j}^{n}}{v_1} + 2\frac{h_a - h_s}{v_3} + \frac{s_i}{v_2}\right) \cdot f_m \tag{6}$$

f_m in eq. (6) represents the detour factor per wind scenario $m \in W$. The actual values are derived from Chu et al. [9], using windspeeds below $11\,\mathrm{m\,s^{-1}}$ as recommended. We computed f_m for seven wind scenarios in TAB 4 with the battery use from table 10 [9], averaging over all wind directions and normalized on $1\,\mathrm{s}$ of flight time. Furthermore, wind scenario $m = 1$ with $0\,\mathrm{m\,s^{-1}}$ and turbulence index 0 is added as a baseline case with $f_m = 1$.

Given the flight endurance $E = 22\,\mathrm{min}$, each rescue mission from i to j is evaluated, so $t_{i,j}^{m,n} \leq E$ from eq. (6) are only classified as accessible:

$$A_{i,j}^{m,n} \cdot (E - t_{i,j}^{m,n} + \epsilon) \cdot M \geq E - t_{i,j}^{m,n} + \epsilon \tag{7}$$

Thus, $A_{i,j}^{m,n} \in \{0,1\}$ is the binary accessibility variable from $i \in F$ to $j \in D$, avoiding the $n \in Z$ and considering $m \in W$, with the Big-M parameter M and an infinitesimally small positive quantity ϵ.

No. $m \in W$	***Windspeed*** $[\mathrm{m\,s^{-1}}]$	***Turbulence index***	***Detour factor*** f_m
1	0	0	1.0
2	3.5	0	1.023
3	10.5	0	1.237
4	3.5	10	1.018
5	10.5	10	1.311
6	3.5	20	1.109
7	10.5	20	2.199

TAB 4. Wind scenarios with detour factors f_m derived from the battery use studied by Chu et al. [9]

3.4. Optimization Model for UAV Hangar Positions

This section describes the FLP model to determine $P \in \mathbb{N}$ optimal UAV hangar locations with maximum accessibility to all hotspots $j \in D$ across all wind scenarios $n \in W$ and all UAS geographic zone scenarios $n \in Z$ while minimizing the respective total flight time. For that, we consider a finite set D of hotspots and finite set F of potential facilities with the binary success variable $A_{i,j}^{m,n} \in \{0,1\}$ from eq. (7) and total flight time $t_{i,j}^{m,n} \in \mathbb{R}+$ from eq. (6), such that:

$$max \sum_{i \in F} \sum_{j \in D} \sum_{m \in W} \sum_{n \in Z} (A_{i,j}^{m,n} - t_{i,j}^{m,n}) \tag{8}$$

With the binary parameter $y_j \in 0,1$ and P facility locations to be established, while $x_{i,j}^{n} \in 0,1$ ensures that each i is connected to only one j:

$$\sum_{i \in F} y_i \leq P \qquad \forall i \in F \tag{9}$$

$$x_{i,j}^{n} \leq y_i \qquad \forall i \in F, j \in D, n \in Z \tag{10}$$

$$\sum_{i \in F} x_{i,j}^{n} \leq 1 \qquad \forall i \in F, j \in D, n \in Z \tag{11}$$

To this end, we process the data of section 3.2 in a georeferenced $5\,\mathrm{m} \times 5\,\mathrm{m}$ grid inside $[51.48°, 51.55°]$ latitude and $[14.04°, 14.20°]$ longitude. Then, the location factors from TAB 1 and 2 identify the solution space for candidate locations. To reduce the computational effort, a spacing of $50\,\mathrm{m}$ between the candidates for UAV hangar locations is chosen, resulting in $|F| = 12569$ candidate locations. The hotspot areas from section 3.2 are processed with a Connected Component labeling, resulting in 11 separate hotspot areas of varying extents across the two lakes. Each hotspot area is represented by hotspot locations using the centroids of a k-means algorithm with k depending on the respective area surface, resulting in a total of $|D| = 19$ hotspot locations. Consequently, a total of $19 \cdot 12569 \cdot 7 \cdot 5 = 8.358 \times 10^6$

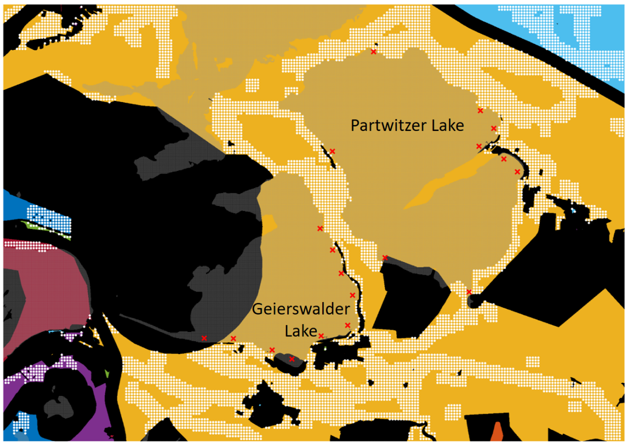

FIG 4. Connected-component labeling of the target area for $n = 5$, indicating all UAV hangar candidate locations (white dots) with valid connection in yellow, and invalid connections in other colors.

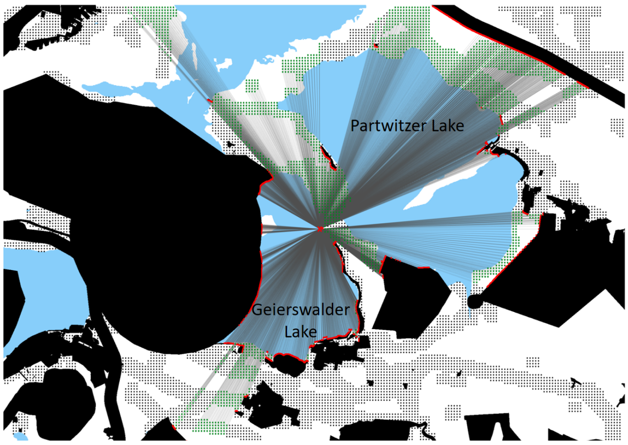

FIG 5. Ray occupancy intersection for finding candidate locations with direct, unrestricted flight paths (green) to one sample hotspot (red dot) to reduce the computational effort of the pathfinding.

path computations for one optimal facility location and $19 \cdot \binom{12569}{2} \cdot 7 \cdot 5 = 5.252 \times 10^{10}$ calculations for two hangar locations is required. Since restriction-free pathfinding with the A* algorithm has a high computational effort, we reduce the number of paths by applying two techniques.

First, we label the discretized binary occupancy grid using a Connected Components algorithm removing all inaccessible candidates due to restrictions. FIG 4 illustrates the method using $n = 5, n \in Z$, as an example. All candidate locations labeled 'yellow' are valid connections to the hotspots, removing invalid candidate locations (e.g., 'purple') from the later pathfinding.

Second, a fast occupancy intersection algorithm checks if straight paths from j to i exist that do not infringe on restricted areas. If this is the case, the shortest path is already found, and the A* computation is not required for this particular combination. FIG 5 illustrates the procedure using $n = 5, n \in Z$, as an example. Green marked location candidates permit direct paths, given one example hotspot at Geierswalder Lake. Red borders show interruptions due to the occupancy envelope, respectively, non-valid direct path.

With these two steps, all UAV hangar candidates without valid connections and with unrestricted straight connections have been identified. Accordingly, only the candidates with the same connected-component label in FIG 4 and intersecting with the occupancy envelope in FIG 5 require calculating a restriction-free path with the A* algorithm in the two-dimensional discretized operation space. Horizontal, vertical, and oblique movements are allowed. The cumulative great circle distance of the georeferenced path nodes along the shortest path from each source to each sink was subsequently calculated, considering geographic areas.

4. RESULTS

Using $P = 1$ and $P = 2$ planned UAV hangar facilities as examples, we demonstrate the resulting optimal locations according to eqs. (8) to (11) and evaluate their performance compared to the remaining candidates. For the shortest path calculation, the two methods described in section 3.4, cf. FIG 4 and 5, predetermine 100% of the distances for $n = 1$, 81.66% for $n = 2$, 70.98% for $n = 3$, 62.31% for $n = 4$ and 44.37% for $n = 5$, resulting in a significant reduction of the computational time. The remaining shortest paths are calculated with an A* algorithm to determine $d_{i,j}^n$ for eq. (6).

FIG 6 shows the accessibility score $A_i \forall i \in F$ derived from the accessibility $A_{i,j}^{m,n}$ from eqs. (8) to (11) normalized over all n and m based on the maximum number of accessible hotspots. $A_i = 0$ indicates that any hotspot cannot be reached over all scenarios m and n, while $A_i = 1$ represents the hangar location with the most accessible hotspots over all scenarios. Different shades of gray indicate the geographic zones depending on the different scenarios n.

Since some hotspots, e.g., $j = 1$, are located inside geographic zones, they cannot be reached from any location candidate in the scenario n containing this particular geographic zone. For $n = 1$, all hotspots are located outside geographical zones, so they can be served as desired. For $n = 2$, one hotspot is inside a geographical zone, reducing the maximum accessible hotspots to 18. In this case, the inaccessible hotspot is removed from the score, resulting in $A_i = 1$ for the best candidates. Analogously, a maximum of $[19, 18, 17, 16, 16]$ hotspots is achievable for all n. Accordingly, for $P = 1$ two potential locations exist that cover the most hotspots across all scenarios $n \in W$ and $m \in Z$. TAB 5 shows the number of hotspots covered for the two candidates.

FIG 7 summarizes A_i per wind scenario m, indicating that the zero- and low-wind cases $m = \{1, 2, 4\}$ provide a very high median accessibility of approx. 75% for all location candidates. Furthermore, the optimal locations

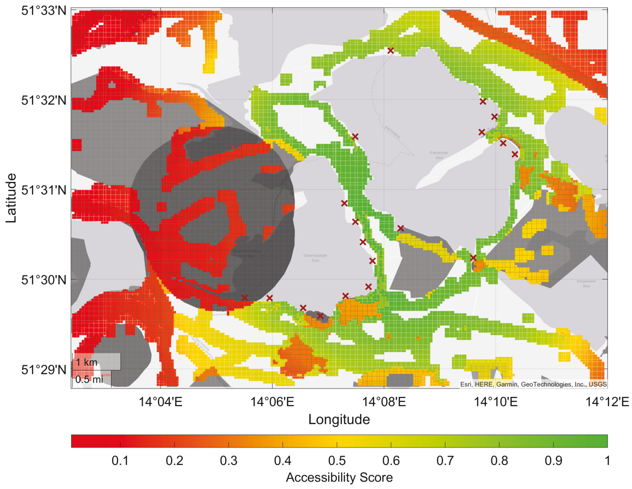

FIG 6. Accessibility score A_i for all UAV hangar location candidates, normalized over all hotspots, geographic zones (gray-shaded areas) and weather scenarios, with $A_i = 1$ for candidates with maximum access to the hotspots

Geographic zone $n \in Z$ \ Wind scenarios $m \in W$: A	1	2	3	4	5	6	7
1	19	19	19	19	19	19	11
2	18	18	18	18	18	18	11
3	17	17	17	17	17	17	10
4	16	16	16	16	16	16	9
5	16	16	16	16	16	16	9

TAB 5. Number of hotspots served by the $P = 1$ optimal UAV hangar locations per wind and geographic zone scenario

for both $P = 1$ and $P = 2$ provide 100% accessibility in all wind scenarios except $m = 7$. In this high-wind-high-turbulence case, the available Endurance E is smaller than a subset j of $t_{i,j}^{5,n}$, so the SAR operation cannot be guaranteed for all hotspots. However, $P = 2$ provides a higher accessibility compared to $P = 1$ in $m = 7$. Consequently, the probability and impact of adverse weather situations should be studied further, as it may justify a third UAV hangar.

For analyzing the SAR performance, we compute the service time $S_{i,j}^{m,n}$ in [s], which is the duration until the search mission ends and the return to the UAV hangar starts. Thus, it indicates the upper bound for the time until the person in distress will be discovered, with:

$$S_{i,j}^{m,n} = \left(\frac{h_a}{v_3} + \frac{d_{i,j}^n}{v_1} + \frac{h_a - h_s}{v_3} + \frac{s_i}{v_2} \right) \cdot f_m \quad (12)$$

FIG 8 summarizes the service times across all $n \in Z$ for all $i \in D$ as a box plot. As indicated by the markers, the $P = 1$ and $P = 2$ optimized locations provide excellent service times compared to all other candidates, significantly below the median and close to the minimum

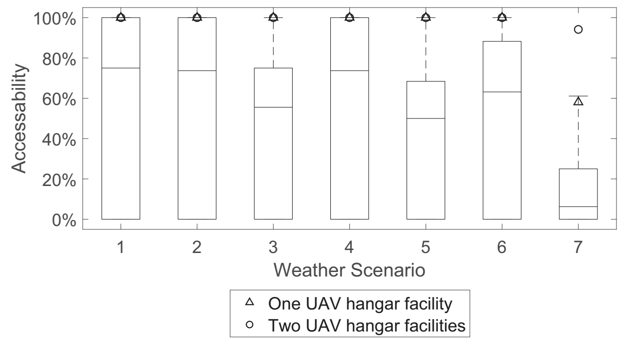

FIG 7. Accessibility score A_i for all location candidates per weather scenario m, indicating 100% accessibility for $P = 1$ and $P = 2$ optimal locations except for $m = 7$

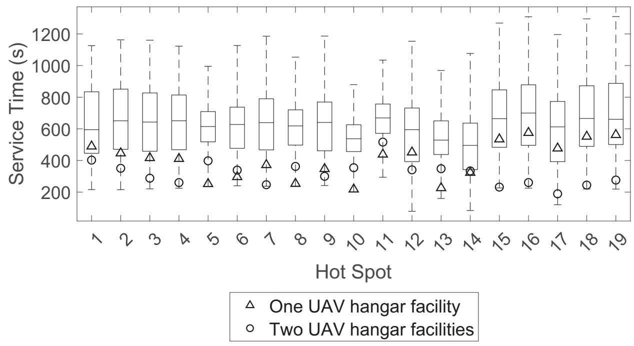

FIG 8. Service time of all location candidates per hotspot, with markers indicating the the optimal UAV hangar locations for $P = 1$ and $P = 2$

for each hotspot. Only hotspots $j = 15$ to $j = 19$, located at the farther side of Lake Partwitz, cf. FIG 9, show a slightly worse service time due to the balanced optimization among all hotspots.

FIG 9 shows the optimal location for $P = 1$, satisfying eqs. (8) to (11), and the shortest flight paths from the optimal facility to all hotspots $j \in D$ while respecting the UAS geographic zones, using $n = 5$ as an example. The heatmap indicates the average service time to all j across all $m \in W$ and $n \in Z$ as a normalized score for all facility candidates with $A_i > 0.9$ indicating near-optimal locations with a slightly inferior result, which may be used as alternatives if the optimal location is not available for building the UAV hangar.

For $P = 2$, 80 possible combinations of candidates have the maximum accessibility score. FIG 10 shows the combination satisfying eq. (8). The plotted paths indicate the hotspot assignment according to eqs. (9) to (11) for $n = 5$ as an example. This assignment is part of the optimization process and represents the shortest service time in each case. However, for operational reasons, the other facility may also serve the hotspot if satisfying eq. (7). Furthermore, the service time eq. (12) is significantly better compared to $P = 1$, especially for hotspots $j = 15$ to $j = 19$, cf. FIG 8.

5. CONCLUSION AND OUTLOOK

We demonstrated a fast and robust method for optimizing UAV hangar locations considering restrictive areas

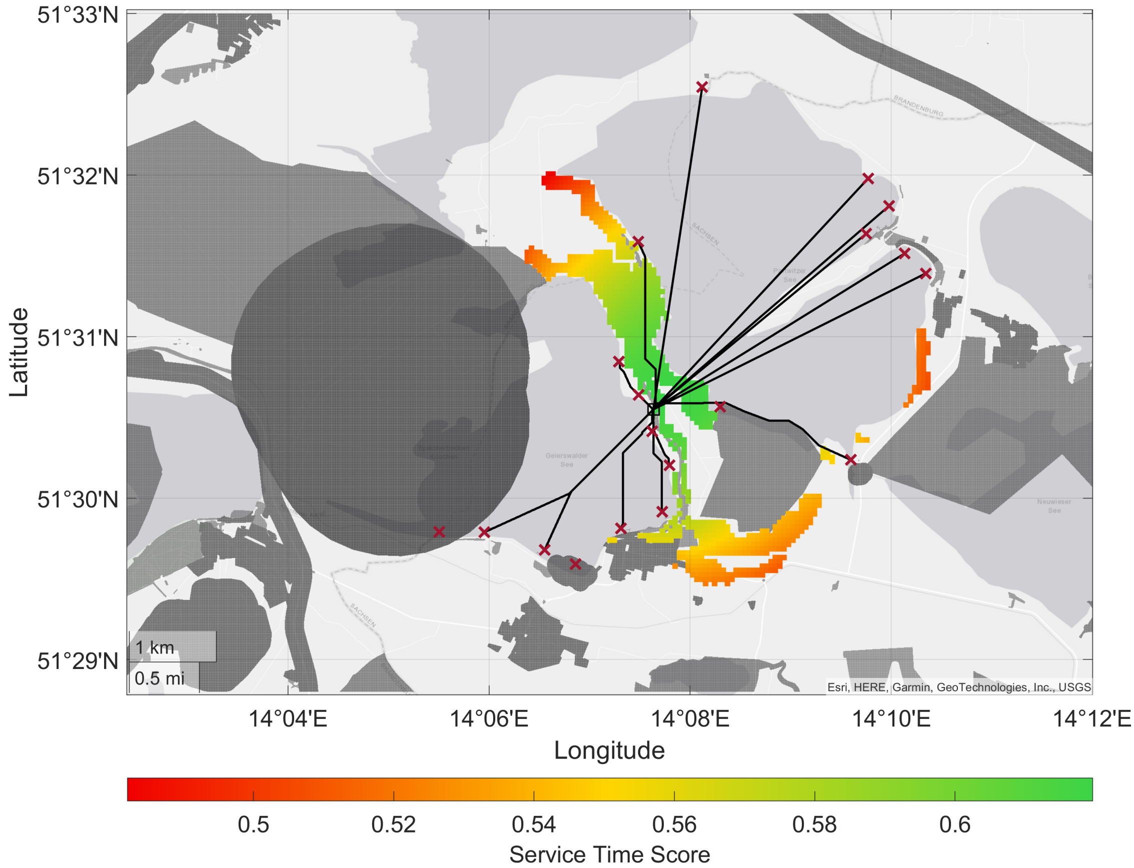

FIG 9. Optimal UAV hangar location for $P = 1$ (square) and the optimal flight paths for $n = 5$ (black) to the hotspots (red) with the restricted areas in gray. The heatmap indicates the service time score for candidates with $A_i > 0.9$, if the optimal site is not available.

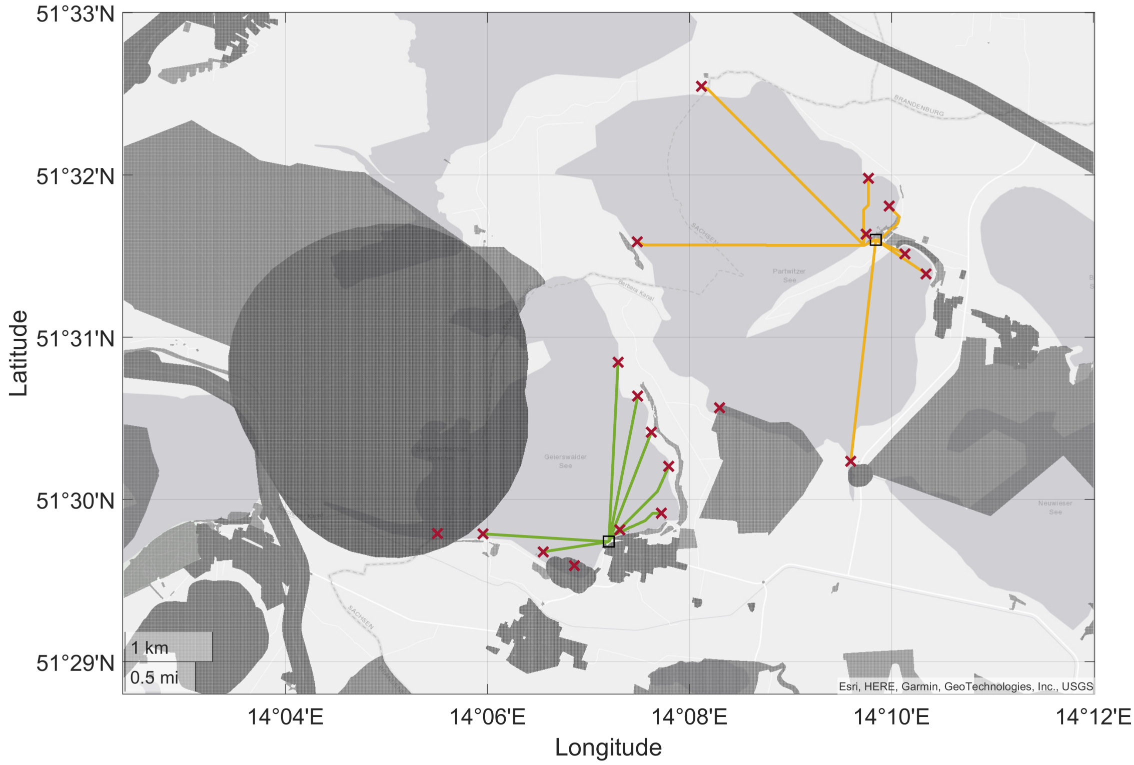

FIG 10. Optimal UAV hangar locations for $P = 2$ (squares) and the optimal flight paths with the allocation to the hangars for $n = 5$ (green and orange) to the hotspots (red) with the restricted areas in gray

and wind scenarios using open-source data. The optimal locations show significantly greater accessibility and lower service time than the other hangar location candidates. Furthermore, the rescue times improved compared to maximum response time regulated for each federal state in Germany. Typically, rescue stations shall be established to reach any emergency site along a public road within $15\,\mathrm{min}$ for 95% of all annual cases, e.g., in Brandenburg [35]. Consequently, emergency services should arrive at the closest public road to the accident site at the lake in about $900\,\mathrm{s}$. Then, additional time is required to reach the shoreline area, which may be difficult to access, and the SAR time in the water. With the optimal UAV hangar locations, average service times over all $n \in Z$ for $m = 1$ of $\bar{S}_{P=1} = 401.69\,\mathrm{s}$ and $\bar{S}_{P=2} = 315.37\,\mathrm{s}$, respectively, were achieved guaranteeing a significant reduction in SAR time. During this time, the UAV will provide a flotation device to the person in distress. Thus, it reacts earlier than required, provides measures to increase survivability, and guides emergency responders to the right location faster. If even faster UAV responses are deemed necessary, a maximum permissible service time may be serve as an additional constraint to our optimization model.

The identified UAV hangar locations are an optimal solution concerning the determined hotspots. Thus, the optimal converage is provided in these hotspot areas. Nevertheless, the RescueFly concept of operations also plans SAR missions outside these hotspot areas. Our concept of hotspots successfully prioritizes areas with high probability of swimming accidents, but it does not exclude the UAV from operating over other parts of the lakes. The accessibility of eq. (7) indicates if the endurance permits these operations.

Next, we plan to integrate a UAV flight performance model for a more precise estimation of the energy consumption, thus, considering the UAV endurance as a dynamic value affected by the weather and other operating conditions. In addition, the RescueFly project partners work on the automated recognition of persons in distress, leading to a more precise definition of the standard SAR mission. Finally, flight demonstrations are planned for the proof of concept.

Acknowledgment

The research presented is part of the project 'RescueFly', number 45ILM1016D, which is funded by the German Federal Ministry for Digital and Transport.

Contact address:

hannes.brassel@tu-dresden.de

References

[1] World Health Organization. Drowning. https://www.who.int/news-room/fact-sheets/detail/drowning, April 2021.

[2] Jahresbericht 2021. Technical report, Deutsche Lebens-Rettungs-Gesellschaft e.V. (DLRG), Bad Nenndorf, 2021.

[3] K. Ajgaonkar, S. Khanolkar, J. Rodrigues, E. Shilker, P. Borkar, and E. Braz. Development of a Lifeguard assist Drone for coastal search and rescue. In *Global Oceans 2020: Singapore – U.S. Gulf Coast*, pages 1–10, October 2020, DOI: 10.1109/IEEECONF38699.2020.9389382.

[4] C. Seguin, G. Blaquière, A. Loundou, P. Michelet, and T. Markarian. Unmanned aerial vehicles (drones) to prevent drowning. *Resuscitation*, 127:63–67, June 2018. ISSN 0300-9572, DOI: 10.1016/j.resuscitation.2018.04.005.

[5] J. Dufek and R. Murphy. Visual pose estimation of USV from UAV to assist drowning victims recovery. In *2016 IEEE International Symposium on Safety, Security, and Rescue Robotics (SSRR)*, pages 147–153, October 2016, DOI: 10.1109/SSRR.2016.7784291.

[6] Z. Liu, H. Chen, Y. Wen, C. Xiao, Y. Chen, and Z. Sui. Mode Design and Experiment of Unmanned Aerial Vehicle Search and Rescue in Inland Waters *. In *2021 6th International Conference on Transportation Information and Safety (ICTIS)*, pages 917–922, October 2021, DOI: 10.1109/ICTIS54573.2021.9798667.

[7] L. Ruetten, P. A. Regis, D. Feil-Seifer, and S. Sengupta. Area-Optimized UAV Swarm Network for Search and Rescue Operations. In *2020 10th Annual Computing and Communication Workshop and Conference (CCWC)*, pages 0613–0618, January 2020, DOI: 10.1109/CCWC47524.2020.9031197.

[8] R. Brühl, H. Fricke, and M. Schultz. Air taxi flight performance modeling and application. In *USA/Europe ATM R&D Seminar*, September 2021.

[9] T. Chu, M. J. Starek, J. Berryhill, C. Quiroga, and M. Pashaei. Simulation and Characterization of Wind Impacts on sUAS Flight Performance for Crash Scene Reconstruction. *Drones*, 5(3):67, September 2021. ISSN 2504-446X, DOI: 10.3390/drones5030067.

[10] L. Lin and M. A. Goodrich. UAV Intelligent Path Planning for Wilderness Search and Rescue. In *2009 IEEE/RSJ International Conference on Intelligent Robots and Systems*, pages 709–714, October 2009, DOI: 10.1109/IROS.2009.5354455.

[11] S. Hayat, E. Yanmaz, T. X. Brown, and C. Bettstetter. Multi-objective UAV path planning for search and rescue. In *2017 IEEE International Conference on Robotics and Automation (ICRA)*, pages 5569–5574, May 2017, DOI: 10.1109/ICRA.2017.7989656.

[12] C. Wang, P. Liu, T. Zhang, and J. Sun. The Adaptive Vortex Search Algorithm of Optimal Path Planning for Forest Fire Rescue UAV. In *2018 IEEE 3rd Advanced Information Technology, Electronic and Automation Control Conference (IAEAC)*, pages 400–403, October 2018, DOI: 10.1109/IAEAC.2018.8577733.

[13] J. Zuo, J. Chen, Z. Li, Z. Li, Z. Liu, and Z. Han. Research on Maritime Rescue UAV Based on Beidou CNSS and Extended Square Search Algorithm. In *2020 International Conference on Communications, Information System and Computer Engineering (CISCE)*, pages 102–106, July 2020, DOI: 10.1109/CISCE50729.2020.00027.

[14] Y. Liang, W. Xu, W. Liang, J. Peng, X. Jia, Y. Zhou, and L. Duan. Nonredundant Information Collection in Rescue Applications via an Energy-Constrained UAV. *IEEE Internet of Things Journal*, 6(2):2945–2958, April 2019. ISSN 2327-4662, DOI: 10.1109/JIOT.2018.2877409.

[15] M. Dakulović, S. Horvatić, and I. Petrović. Complete Coverage D* Algorithm for Path Planning of a Floor-Cleaning Mobile Robot. *IFAC Proceedings Volumes*, 44(1):5950–5955, January 2011. ISSN 1474-6670, DOI: 10.3182/20110828-6-IT-1002.03400.

[16] P.-F. Xu, Y.-X. Ding, and J.-C. Luo. Complete Coverage Path Planning of an Unmanned Surface Vehicle Based on a Complete Coverage Neural Network Algorithm. *Journal of Marine Science and Engineering*, 9(11):1163, November 2021. ISSN 2077-1312, DOI: 10.3390/jmse9111163.

[17] Y. Sun, Q. Tan, C. Yan, Y. Chang, X. Xiang, and H. Zhou. Multi-UAV Coverage through Two-Step Auction in Dynamic Environments. *Drones*, 6(6):153, June 2022. ISSN 2504-446X, DOI: 10.3390/drones6060153.

[18] L. Qingqing, J. Taipalmaa, J. P. Queralta, T. N. Gia, M. Gabbouj, H. Tenhunen, J. Raitoharju, and T. Westerlund. Towards Active Vision with UAVs in Marine Search and Rescue: Analyzing Human Detection at Variable Altitudes. In *2020 IEEE International Symposium on Safety, Security, and Rescue Robotics (SSRR)*, pages 65–70, November 2020, DOI: 10.1109/SSRR50563.2020.9292596.

[19] P. Rudol and P. Doherty. Human Body Detection and Geolocalization for UAV Search and Rescue Missions Using Color and Thermal Imagery. In *2008 IEEE Aerospace Conference*, pages 1–8, March 2008, DOI: 10.1109/AERO.2008.4526559.

[20] M. B. Bejiga, A. Zeggada, A. Nouffidj, and F. Melgani. A Convolutional Neural Network Approach for Assisting Avalanche Search and Rescue Operations with UAV Imagery. *Remote Sensing*, 9(2):100, February 2017. ISSN 2072-4292, DOI: 10.3390/rs9020100.

[21] E. Lygouras, N. Santavas, A. Taitzoglou, K. Tarchanidis, A. Mitropoulos, and A. Gasteratos. Unsupervised Human Detection with an Embedded Vision System on a Fully Autonomous UAV for Search and Rescue Operations. *Sensors*, 19(16):3542, January 2019. ISSN 1424-8220, DOI: 10.3390/s19163542.

[22] V. A. Feraru, R. E. Andersen, and E. Boukas. Towards an Autonomous UAV-based System to Assist Search and Rescue Operations in Man Overboard Incidents. In *2020 IEEE International Symposium on Safety, Security, and Rescue Robotics (SSRR)*, pages 57–64, November 2020, DOI: 10.1109/SSRR50563.2020.9292632.

[23] C. Liu and T. Szirányi. Real-Time Human Detection and Gesture Recognition for On-Board UAV Rescue. *Sensors*, 21(6):2180, January 2021. ISSN 1424-8220, DOI: 10.3390/s21062180.

[24] S. Wang, Y. Han, J. Chen, Z. Zhang, G. Wang, and N. Du. A Deep-Learning-Based Sea Search and Rescue Algorithm by UAV Remote Sensing. In *2018 IEEE CSAA Guidance, Navigation and Control Conference (CGNCC)*, pages 1–5, August 2018, DOI: 10.1109/GNCC42960.2018.9019134.

[25] G. Cornuejols, G. Nemhauser, and L. Wolsey. The uncapacitated, facility location problem. *Discrete Location Theory*, page 119–171, 1990.

[26] D. Shmoys. Approximation algorithms for facility location problems. *Proceedings of the 3rd International Workshop on Approximation Algorithms for Combinatorial Optimization*, page 27–33, 2000.

[27] V. Arya, N. Garg, R. Khandekar, A. Meyerson, K. Munagala, and V. Pandit. Local search heuristic for k-median and facility location problems. In *Proceedings of the Thirty-Third Annual ACM Symposium on Theory of Computing*, STOC '01, pages 21–29, New York, NY, USA, July 2001. Association for Computing Machinery. ISBN 978-1-58113-349-3, DOI: 10.1145/380752.380755.

[28] S. Ahmadian and C. Swamy. Improved approximation guarantees for lower-bounded facility location. *CoRR*, abs/1104.3128, 2011, DOI: 10.48550/arXiv.1104.3128.

[29] T. Zhu, S. D. Boyles, and A. Unnikrishnan. Two-stage robust facility location problem with drones. *Transportation Research Part C: Emerging Technologies*, 137:103563, 2022. ISSN 0968-090X, DOI: 10.1016/j.trc.2022.103563.

[30] J. Lynskey, K. Thar, T. Oo, and C. S. Hong. Facility location problem approach for distributed drones. *Symmetry*, 11:118, 01 2019, DOI: 10.3390/sym11010118.

[31] Commission Implementing Regulation (EU) 2019/947 of 24 May 2019 on the rules and procedures for the operation of unmanned aircraft, May 2019.

[32] Luftverkehrs-Ordnung vom 29. Oktober 2015 (BGBl. I S. 1894), zuletzt geändert durch Artikel 2 des Gesetzes vom 14. Juni 2021 (BGBl. I S. 1766).

[33] Regulation (EU) 2018/1139 of the European Parliament and of the Council of 4 July 2018 on common rules in the field of civil aviation and establishing a European Union Aviation Safety Agency [...], July 2018.

[34] L. E. van Dyck, R. Kwitt, S. J. Denzler, and W. R. Gruber. Comparing Object Recognition in Humans and Deep Convolutional Neural Networks—An Eye Tracking Study. *Frontiers in Neuroscience*, 15, 2021. ISSN 1662-453X, DOI: 10.3389/fnins.2021.750639.

[35] Gesetz über den Rettungsdienst im Land Brandenburg (Brandenburgisches Rettungsdienstgesetz - BbgRettG) vom 14. Juli 2008.